Theory of resonant X-ray emission spectroscopy

A. Kotani

Institute for Solid State Physics, University of Tokyo, Kashiwanoha, Kashiwa, Chiba 277-8581, Japan.
E-mail: kotani@issp.u-tokyo.ac.jp

A short review is presented of recent topics in resonant X-ray emission spectroscopy (RXES), especially of the polarization dependence of RXES in d and f electron systems. Polarization-dependent RXES provides important information on the symmetry of electronic states. A scattering-angle dependence in the fluorescence yield of rare-earth metals, RXES in polarized and depolarized configurations of TiO_2, and the magnetic circular dichroism in RXES of ferromagnetic systems are discussed together with typical experimental data.

Keywords: resonant X-ray emission; polarization dependence; rare-earth metals; transition-metal compounds.

1. Introduction

Resonant X-ray emission spectroscopy (RXES) is one of the most powerful tools in solid-state spectroscopy with synchrotron radiation (Kotani & Shin, 2000). In this paper we report theoretical calculations on the polarization dependence of RXES in d and f electron systems, such as rare-earth metals and transition-metal compounds, together with their experimental results. Using synchrotron radiation with an undulator beamline, the incident photon is polarized linearly or circularly in RXES experiments. However, it is very difficult to detect the polarization of the emitted photon directly.

The polarization-dependent RXES is described theoretically by the coherent second-order optical formula in the form

$$F_{\alpha,\beta}(\Omega,\omega)=\sum_j\left|\sum_i\frac{\langle j|T_\alpha|i\rangle\langle i|T_\beta|g\rangle}{E_g+\Omega-E_i-i\Gamma_i}\right|^2\times\delta(E_g+\Omega-E_j-\omega),\qquad(1)$$

where Ω and ω are, respectively, the energies of the incident and emitted photons with polarization directions β and α; $|g\rangle$, $|i\rangle$ and $|j\rangle$ are initial, intermediate and final states of the material system, respectively, and E_g, E_i and E_j are their energies. The operator T represents the optical dipole transition, and Γ_i is the spectral broadening due to the core-hole lifetime in the intermediate state. Tanaka & Kotani (1993) performed, before experimental observations, theoretical calculations of F_{xx} and F_{zx} in the Cu $2p\rightarrow3d\rightarrow2p$ RXES of La_2CuO_4, where the crystalline c axis is taken in the z direction. They showed that the polarization dependence of RXES provides important information on the symmetry of electronic states.

A few years after the theoretical calculation, $F_{\alpha,\beta}$ of La_2CuO_4 was observed experimentally by using a sophisticated geometrical arrangement where a spectrometer can be rotated around the incident beam axis and a sample can also be rotated around its surface normal (Duda, 1996; Duda *et al.*, 1998). Unfortunately, the resolution is not very good, but the theoretical and experimental results are in fair agreement within the experimental resolution.

More recently, polarization-dependent RXES has been studied more precisely, without detecting the polarization of the emitted photon, by switching the experimental geometry (polarized and depolarized configurations defined later) or by changing the scattering angle.

In this paper three typical examples are presented: scattering-angle dependence (§2), polarized and depolarized configurations (§3), and magnetic circular dichroism (§4) in RXES.

2. Scattering-angle dependence in fluorescence yield of rare-earth metals

We take the incident photon polarization in the z direction and denote a scattering angle by θ, as shown in Fig. 1. The polarization of the emitted photon is not detected. Then the RXES spectrum is expressed as (Nakazawa *et al.*, 1998)

$$F(\Omega,\omega)=\sum_q\sum_j\left|\sum_i\frac{\langle j|C_q^{(1)}|i\rangle\langle i|C_0^{(1)}|g\rangle}{E_g+\Omega-E_i-i\Gamma_i}\right|^2A_q(\theta)\times\delta(E_g+\Omega-E_j-\omega),\qquad(2)$$

where $C_q^{(k)}$ is defined by

$$C_q^{(k)}=[4\pi/(2k+1)]^{1/2}Y_{kq},\qquad(3)$$

with spherical harmonics Y_{kq}, and the angle-dependent factor $A_q(\theta)$ is given by

$$A_q(\theta)=\begin{cases}\frac{1}{2}(1+\sin^2\theta) & q=1,-1\\ \cos^2\theta & q=0\end{cases}.\qquad(4)$$

Experimental observations of the θ dependence of RXES were made by Pompa *et al.* (1997) for the fluorescence yield (FY) of $3d\rightarrow4f\rightarrow3d$ RXES in La and Sm metals, instead of the RXES itself. FY is the spectroscopy where the intensity of RXES integrated over the emitted photon energy is measured as a function of the incident photon energy. The results are shown as dots in Figs. 2(a) and 2(b). It is found that in La the intensity of FY changes drastically with θ, but the spectral shape of FY is unchanged. In Sm, on the other hand, the change in the intensity is less dramatic but the spectral shape changes with θ.

Theoretical calculations of these FY spectra were performed by Nakazawa *et al.* (1998). From (2), the spectrum of FY is given by

$$F_{\rm FY}(\Omega)=\int{\rm d}\omega\;F(\Omega,\omega)=\sum_q f_q(\Omega)\,A_q(\theta),\qquad(5)$$

where

$$f_q(\Omega)=\sum_j\left|\sum_i\frac{\langle j|C_q^{(1)}|i\rangle\langle i|C_0^{(1)}|g\rangle}{E_g+\Omega-E_i-i\Gamma_i}\right|^2.\qquad(6)$$

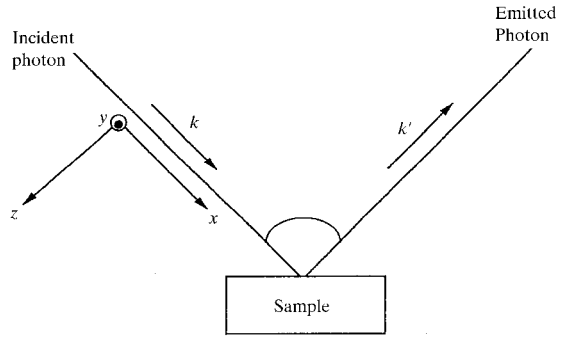

Figure 1
Geometrical arrangement and coordinate axes in the calculation of RXES and FY.

Since the spectral structure of RXES in rare-earth metals is mainly determined by the intra-atomic multiplet structure, the calculation was made with a free-ion model. The calculated results are shown as solid curves in Figs. 2(*a*) and 2(*b*). The theoretical and experimental results are in good agreement with each other. Nakazawa *et al.* (1998) discussed the reason for the angle dependence of FY for La and Sm. For La, FY intensity decreases rapidly as θ increases. Since the initial and final electronic configuration of La^{3+} is $4f^0$ with $J = 0$, only the component $q = 0$ contributes to the FY intensity (note that $F_{zz} \neq 0$ and $F_{xz} = F_{yz} = 0$ in this case), which is proportional to $\cos^2\theta$ as seen from (4).

To understand the angle dependence of FY for Sm, the calculated results of $f_q(\Omega)$ [given by (6)] for $q = 0$ (caused by the diagonal component F_{zz} of RXES) and $q = \pm 1$ (caused by off-diagonal components F_{xz} and F_{yz}) are shown in Fig. 3 for Sm. It is seen that f_0 and $f_{\pm 1}$ for Sm are much different both in their intensity and in their spectral shape. With the change of the angle θ, the weight between f_0 and $f_{\pm 1}$ is changed, so that the angle dependence of FY is understood.

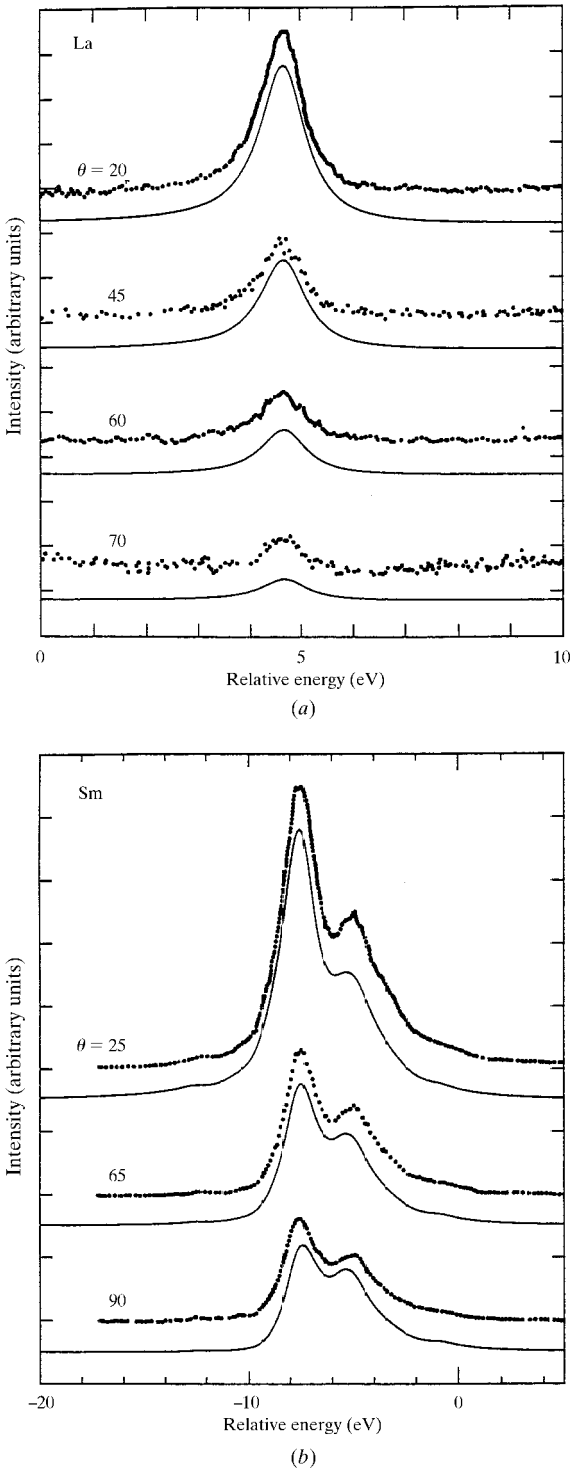

Figure 2
Calculated (line) and experimental (dots) results of the scattering-angle-dependent FY for (*a*) La^{3+} and (*b*) Sm^{3+}.

3. RXES in polarized and depolarized configurations of TiO_2

Let us consider the geometrical configuration shown in Fig. 1. The angle θ between the incident and emitted photon directions is fixed at 90°, and the incident photon polarization is taken in either the y or the z direction, which is denoted by the 'polarized' or 'depolarized' configuration, respectively. The polarization of the emitted photon is not detected. In these two configurations the spectra of RXES are expressed, from (2), as

$$F(\Omega, \omega) = \begin{cases} F_{xy}(\Omega, \omega) + F_{yy}(\Omega, \omega) & \text{(polarized)} \\ F_{xz}(\Omega, \omega) + F_{yz}(\Omega, \omega) & \text{(depolarized)} \end{cases}. \qquad (7)$$

The calculation of the Ti $2p \rightarrow 3d \rightarrow 2p$ RXES of TiO_2 was made by Matsubara *et al.* (2000, 2001) with a TiO_6 cluster model with O_h symmetry. The results are shown in Fig. 4 (lower panel), where the incident photon energy is taken at the positions *a*–*h* in the XAS spectrum (upper panel), and the RXES spectra are plotted as a function of the emitted photon energy with the elastic (Rayleigh) scattering line as the origin. The spectral structure is divided into three categories: (1) elastic line at 0 eV, (2) inelastic spectra at 7 and 9 eV, and (3) inelastic line at 14 eV. The mechanism of these spectra can be explained by the energy-level scheme shown in Fig. 5. TiO_2 is nominally in the d^0 state, but actually the d^0 configuration is strongly mixed with a charge-transferred $d^1\underline{L}$ configuration by the covalency hybridization, where $\underline{L}$ denotes a hole in the ligand state (O $2p$ molecular orbit). The ground state is the bonding state between the d^0 and $d^1\underline{L}$ configurations, and the anti-bonding state is located about 14 eV above the ground state. Both bonding and anti-bonding states

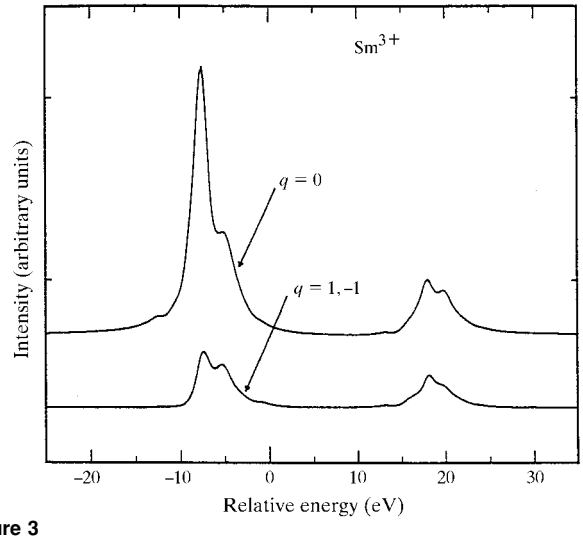

Figure 3
Calculated results of FY for Sm^{3+}, which is decomposed into the polarization component of the emitted X-ray.

are specified by an irreducible representation A_{1g} of the O_h symmetry group, because their symmetry is the same as the d^0 state. In addition to these states, there are non-bonding $3d^1\underline{L}$ states with A_{2g}, T_{1g}, T_{2g}, E_g,... symmetries about 7–9 eV above the ground state. When a Ti $2p$ electron is excited to the $3d$ state by the incident photon, we have $2p^5 3d^1$ and $2p^5 3d^2\underline{L}$ configurations, which are mixed strongly by the covalency hybridization. The main peak of the Ti $2p$ XAS corresponds to the bonding state between the $2p^5 3d^1$ and $2p^5 3d^2\underline{L}$ configurations, while the satellite corresponds to the anti-bonding state between them. X-ray absorption is almost forbidden in the non-bonding states. In Fig. 5 we disregard the effects of the spin–orbit splitting of the $2p$ states and the crystal field splitting of the $3d$ states, for simplicity. If we take into account these effects, the main peak (and also the satellite) splits into four peaks, as seen in Fig. 4.

The resonantly excited intermediate states, which correspond to the main line and the satellite of XAS, decay radiatively to each of the final states of RXES, *i.e.* the bonding, non-bonding and anti-bonding states. The categories (1), (2) and (3) of RXES spectra correspond to the bonding, non-bonding and anti-bonding final states, respectively. The spectrum (3) occurs for the incident photon energy tuned to the satellite of the XAS spectrum. This is because the XAS satellite corresponds to the anti-bonding intermediate state of RXES, so that it enhances dramatically the intensity of the anti-bonding final state (3). The spectra (1) and (3) are allowed only for the polarized configuration, while the spectrum (2) is allowed for both polarized and depolarized configurations.

Let us consider the mechanism of the polarization dependence of the RXES spectra. It is easily shown from (7) and group theoretical consideration that the final states with A_{1g}, T_{1g}, T_{2g} and E_g irreducible representations are allowed for the polarized configuration, whereas those with only T_{1g} and T_{2g} irreducible representations are allowed for the depolarized configuration. Therefore, the elastic peak (bonding state) and the 14 eV inelastic peak (anti-bonding state) are allowed for the polarized configuration, but they are forbidden for the depolarized configuration. The non-bonding states are allowed both for the polarized and depolarized configurations.

Very recently, experimental measurements of RXES for TiO_2 have been made by Harada *et al.* (2000) for the polarized and depolarized configurations. The result is shown in Fig. 6. The three categories of RXES spectra (1)–(3) are clearly seen, in addition to the spectra indicated by vertical bars, which are absent in our TiO_6 cluster-model calculation (Fig. 4) but are explained as originating from the effect of the periodic arrangement of the Ti ions (Idé & Kotani, 1998). The elastic scattering peak at 0 eV (category 1) and the inelastic one at 14 eV (category 3) are allowed only for the polarized configuration, and the intensity of the 14 eV peak is dramatically enhanced when the incident photon energy is tuned to the satellite of the XAS spectrum. Near the middle of the elastic (0 eV) and inelastic (14 eV) scattering peaks, there are inelastic scattering spectra (category 2) which are allowed both for the polarized and depolarized configurations. These results are in good agreement with the calculated ones.

It is to be remarked that the reason that the elastic and the 14 eV inelastic lines are forbidden for the depolarized configuration is that the off-diagonal components, F_{xz} and F_{yz}, vanish if both initial and final states of RXES are the non-degenerate A_{1g} state. In other words, if the initial and final states of the material system are the same, the polarizations of the incident and emitted photons should also be the same, because the angular momentum of the total system (including the photon and the material) is conserved. The reason that the FY of La vanishes for $\theta = 90^\circ$ is also essentially the same.

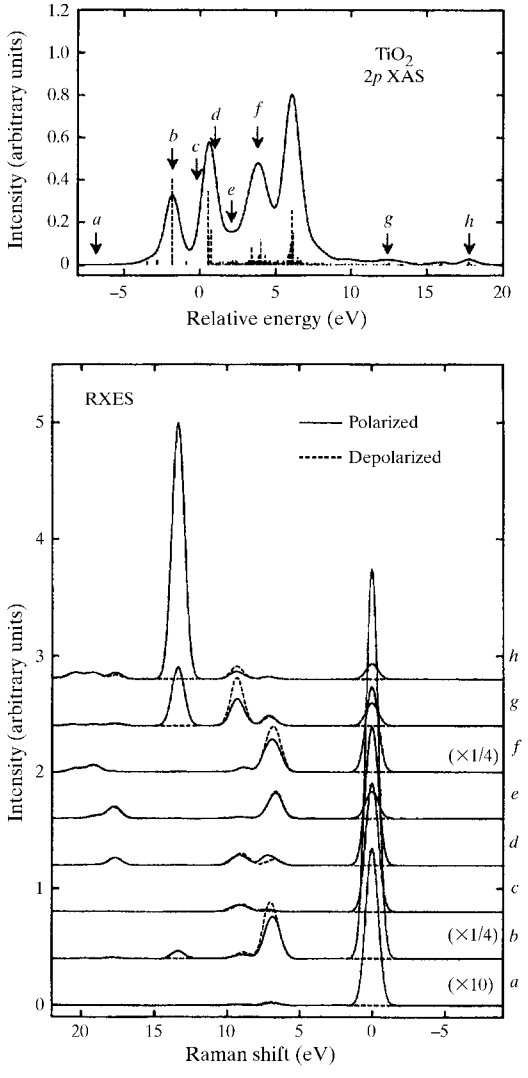

Figure 4
Calculated results of Ti $2p$ XAS and $2p \rightarrow 3d \rightarrow 2p$ RXES of TiO_2 using the TiO_6 cluster model.

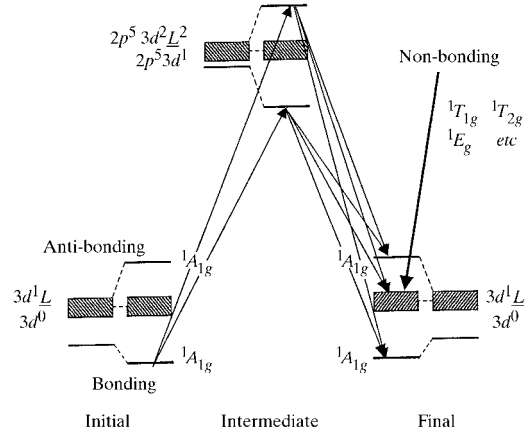

Figure 5
Schematic representation of the Ti $2p \rightarrow 3d \rightarrow 2p$ RXES of TiO_2 using the TiO_6 cluster model.

4. MCD in RXES of ferromagnetic systems

Another interesting phenomenon on the polarization dependence of RXES is the magnetic circular dichroism (MCD) in ferromagnetic systems. We consider the situation where a photon with circular polarization (+ or − helicity) is incident on the sample with an angle φ from the sample surface normal, and the emitted photon is detected with an angle φ' from the surface normal without analyzing the polarization, where the surface normal is perpendicular to the magnetization of the sample, and all the directions of incident and emitted photons, surface normal and the magnetization are in the same plane. Then the MCD of RXES, *i.e.* the difference of RXES for the incident photons with + and − helicities, is given by

$$\begin{aligned}\Delta F_{\rm MCD}(\Omega,\omega) = & -\tfrac{1}{2}\sin\varphi\left[\left(1+\sin^2\varphi'\right)\right.\\ & \times\left(F_{1-1}+F_{-1-1}-F_{11}-F_{-11}\right)\\ & \left.+\,2\cos^2\varphi'(F_{0-1}-F_{01})\right],\end{aligned} \tag{8}$$

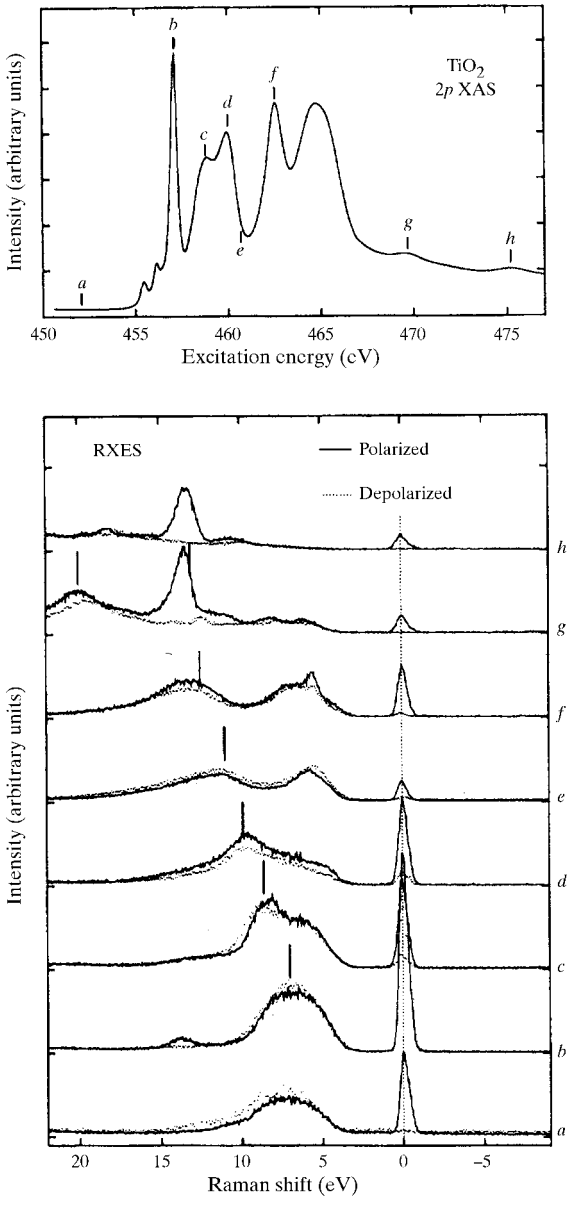

Figure 6
Experimental results of Ti $2p$ XAS and $2p \rightarrow 3d \rightarrow 2p$ RXES of TiO_2.

where $F_{q'q}$ is defined by

$$F_{q'q} = \sum_j \left| \sum_i \frac{\langle j|C^{(1)}_{q'}|i\rangle\langle i|C^{(1)}_{q}|g\rangle}{E_g+\Omega-E_i-i\Gamma_i} \right|^2 \delta(E_g+\Omega-\omega-E_j),$$

with the polar axis [for $C^{(1)}_q$] taken in the direction of the magnetization.

An example is shown in Fig. 7. Here, the experimental data (dots) (Krisch *et al.*, 1996; de Groot *et al.*, 1997) are shown for the X-ray emission and its MCD for ferromagnetic Gd metal, where a $2p_{3/2}$ core electron is excited to a high-energy continuum (instead of the excitation near to the threshold) and a $3d_{5/2}$ electron makes a radiative transition to the $2p_{3/2}$ state. The angles φ and φ' are taken as 60° and 30°, respectively. The calculated results (de Groot *et al.*, 1997) with a Gd^{3+} ion model are also shown by the solid curves. The agreement with the experimental results is good. Experiments and calculations similar to this but for the 4*d* core level (instead of the 3*d* level) were also made by Krisch *et al.* (1996) and by de Groot *et al.* (1997). Also, similar calculations of normal X-ray emission spectroscopy (NXES) and MCD were made by Jo & Tanaka (1998) for both 3*d* and 4*d* core levels of Nd^{3+}, Gd^{3+} and Dy^{3+} ions.

Finally, it is to be mentioned that the MCD of RXES, where the incident photon energy is tuned to the absorption threshold, is a more interesting subject. Krisch *et al.* (1996) and Iwazumi *et al.* (1997) observed the MCD of Gd $3d_{5/2} \rightarrow 2p_{3/2}$ RXES in the $2p_{3/2}$ excitation threshold. The data should include important information on the magnetic polarization of both ground and excited states. Since the final state of XAS is the same as the intermediate state of RXES, a

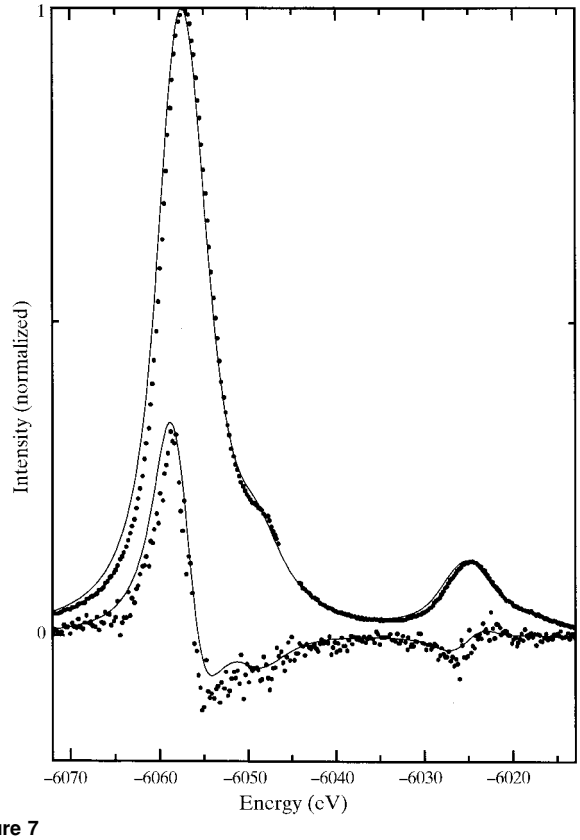

Figure 7
Gd $3d$–$2p_{3/2}$ X-ray emission spectrum (upper) and its MCD (lower) under the excitation of a $2p_{3/2}$ core electron to a high-energy continuum by circular polarized incident X-rays. Solid curves and dots are the calculated and experimental results, respectively.

theoretical analysis of these data of MCD in RXES should be a critical test of the validity of possible mechanisms proposed for the MCD in XAS, and some study along this line is now in progress (Fukui *et al.*, 2001).

The author would like to thank Professor K. Okada, Professor I. Harada, Professor S. Tanaka, Dr H. Ogasawara, Dr T. Uozumi, Dr M. Nakazawa, Dr T. Idé, Dr K. Fukui, Mr M. Matsubara, Dr F. M. F. de Groot, Professor S. Shin, Dr Y. Harada, Dr L. C. Duda, Dr P. Lagarde and Dr M. Pompa, for collaborations and discussions. This work was partially supported by a Grant-in-Aid for Scientific Research from the Ministry of Education, Science, Culture and Sports in Japan.

References

Duda, L. C. (1996). Thesis, Uppsala University, Sweden.
Duda, L. C., Dräger, G., Tanaka, S., Kotani, A., Guo, J., Heumann, D., Bocharov, S., Wassdahl, N. & Nordgren, J. (1998). *J. Phys. Soc. Jpn*, **67**, 416–419.
Fukui, K., Ogasawara, H., Harada, I. & Kotani, A. (2001). *J. Synchrotron Rad.* **8**, 407–409.
Groot, F. M. F. de, Nakazawa, M., Kotani, A., Krisch, M. H. & Sette, F. (1997). *Phys. Rev. B*, **56**, 7285–7292.
Harada, Y., Kinugasa, T., Eguchi, R., Matsubara, M. & Kotani, A. (2000). *Phys. Rev. B*, **61**, 12854–12859.
Idé, T. & Kotani, A. (1998). *J. Phys. Soc. Jpn*, **67**, 3621–3629.
Iwazumi, T., Kobayashi, K., Kishimoto, S., Nakamura, T., Nanao, S., Ohshima, D., Katano, R. & Isozumi, Y (1997). *Phys. Rev. B*, **56**, 14267–14270.
Jo, T. & Tanaka, A. (1998). *J. Phys. Soc. Jpn*, **67**, 1457–1465.
Kotani, A. & Shin, S. (2000). *Rev. Mod. Phys.* To be published.
Krisch, M. H., Sette, F., Bergmann, U., Masciovecchio, C., Verbeni, R., Goulon, J., Caliebe, W. & Kao, C. C. (1996). *Phys. Rev. B*, **54**, 12673–12676.
Matsubara, M., Uozumi, T. & Kotani, A. (2001). *J. Synchrotron Rad.* **8**, 393–395.
Matsubara, M., Uozumi, T., Kotani, A., Harada, Y. & Shin, S. (2000). *J. Phys. Soc. Jpn*, **69**, 1558–1565.
Nakazawa, M., Ogasawara, H., Kotani, A. & Lagarde, P. (1998). *J. Phys. Soc. Jpn*, **67**, 323–331.
Pompa, M., Flank, A. M., Lagarde, P., Rife, J., Stekhin, I., Nakazawa, M., Ogasawara, H. & Kotani, A. (1997). *Phys. Rev. B*, **56**, 2267–2272.
Tanaka, S. & Kotani, A. (1993). *J. Phys. Soc. Jpn*, **62**, 464–467.